Supporting Information

Removal of Differential Capacitive Interferences in Fast-Scan Cyclic Voltammetry

Justin A. Johnson[†], Caddy N. Hobbs[†], and R. Mark Wightman[*,†,‡]

[†]Department of Chemistry and [‡]Neuroscience Center and Neurobiology Curriculum, University of North Carolina at Chapel Hill, Chapel Hill, North Carolina 27599-3290, United States

*Corresponding Author: Phone: 919-962-1472. E-mail: rmw@unc.edu

Supporting Information Available:

Figure S1: Background-subtracted FSCV signals for Na^+ and Ca^{2+} concentration changes in phosphate-buffered saline.

Figure S2: FSCV signals seen during ionic concentration changes in TRIS buffer.

Figure S3: Background-subtracted FSCV signals for dopamine concentration changes in PBS and TRIS buffer.

Figure S4: Results of one-phase exponential decay fit to current response to 40 mV voltage step at carbon-fiber microelectrode.

Figure S5: Voltage-dependent psuedocapacitance determined from small amplitude CVs at carbon-fiber microelectrode.

Figure S6: Power spectra for a triangular voltage wave and typical impulse response at carbon-fiber microelectrode.

Figure S7: Effect of step size on prediction for different voltage step amplitudes (20-200 mV) using a low-pass voltage filter (cut-off frequency of 25 kHz) and sampling frequency of 300 kHz.

Figure S8: Model-simulated currents for the components of the carbon-fiber double layer.

Supplemental discussion concerning the derivation of model for simulation of background currents at carbon-fiber microelectrodes.

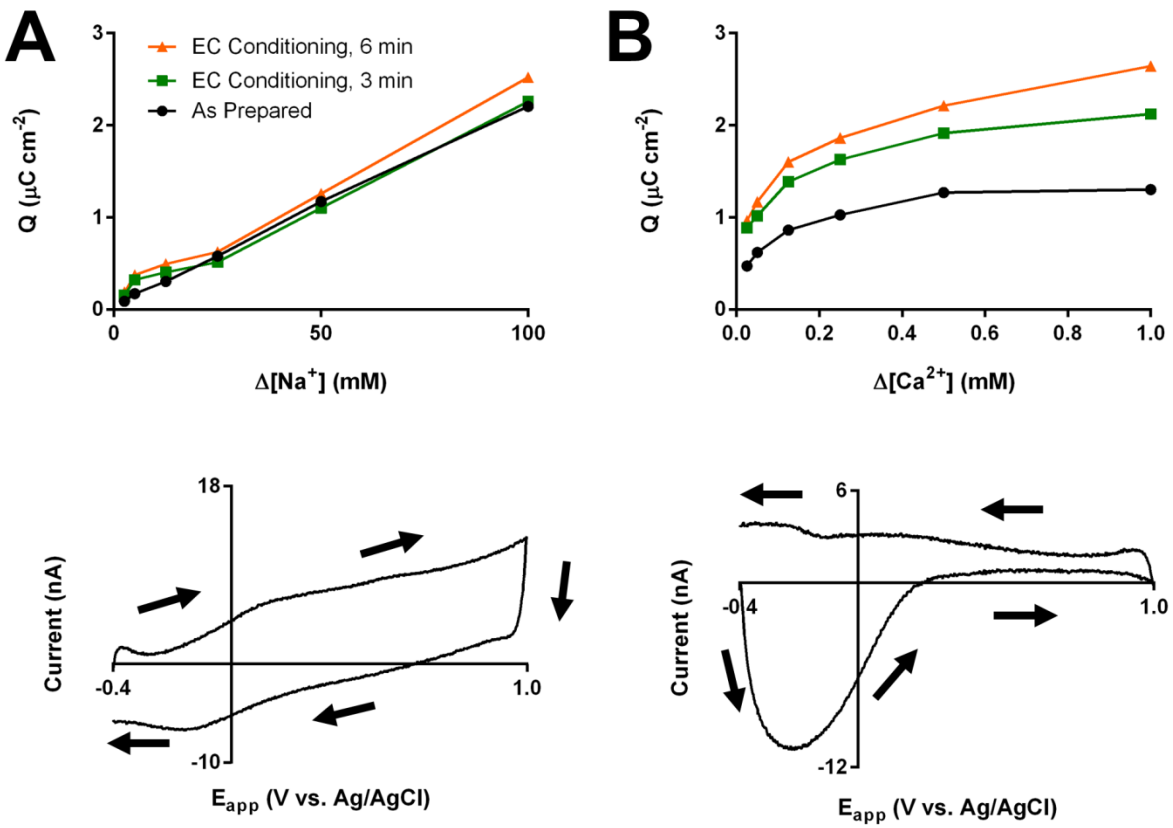

Figure S-1. Background-subtracted FSCV signals for Na^+ and Ca^{2+} concentration changes in phosphate-buffered saline. Adsorption curves (2.5-100 mM, top) for differing lengths of electrochemical conditioning (as prepared, black; 3-minute conditioning, green; 6-minute conditioning, orange) and representative background-subtracted CV (100 mM, bottom) for sodium injections (A) and calcium (B) injections.

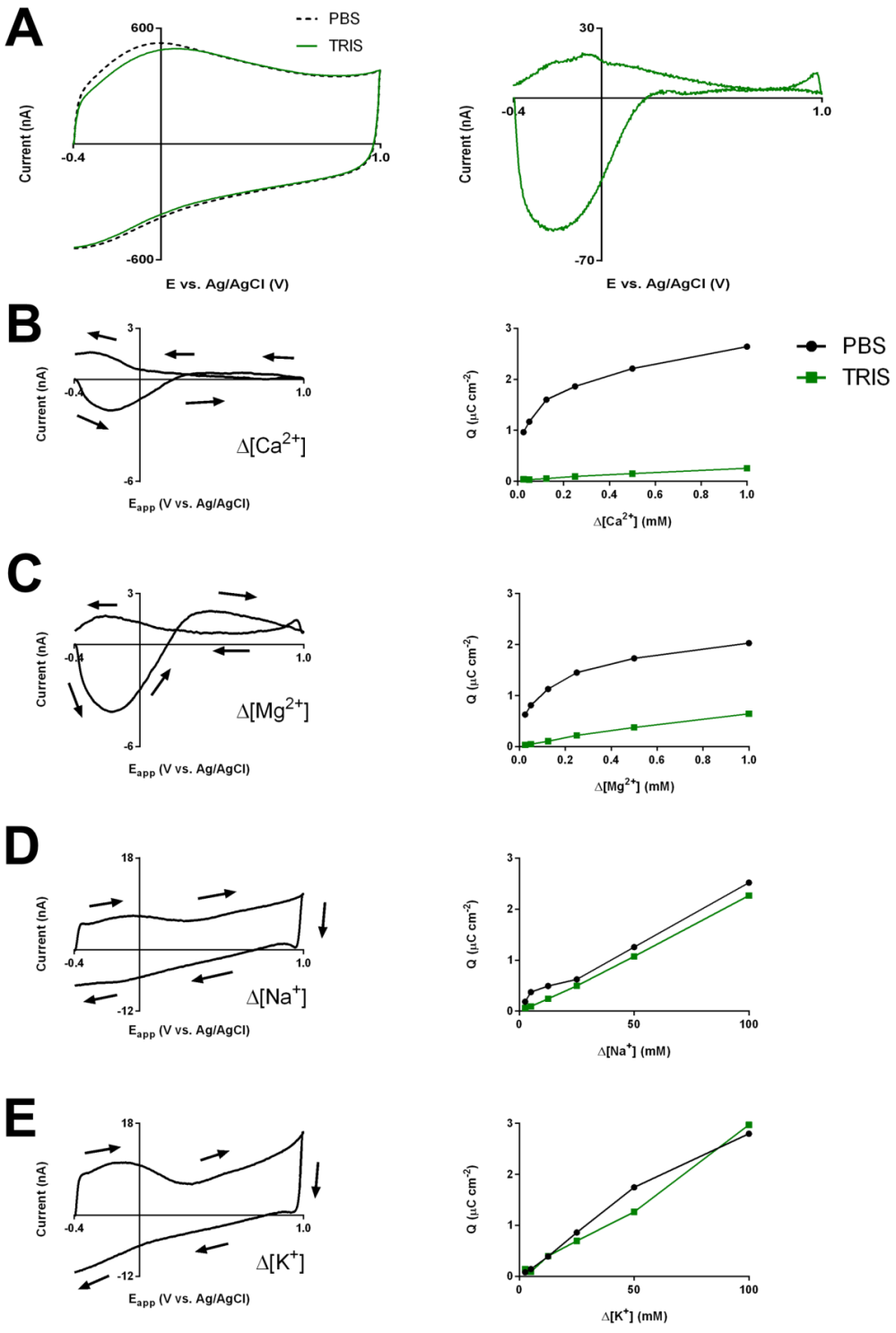

Figure S-2. FSCV signals seen during ionic concentration changes in TRIS buffer. (A) Background CVs (left, -0.4-1.0 V vs Ag/AgCl, 400 V/s, 10 Hz) in PBS (dashed black) and after injection of TRIS buffer (green), as well as the background-subtracted CV (right, TRIS-PBS). (B-E) Representative background-subtracted CVs (left) and adsorption curves (right, obtained from integration of full CV; black – PBS, green - TRIS) for Ca^{2+} (B), Mg^{2+} (C), Na^{+} (D), and K^{+} (E). The PBS data is that from Figures 1 and S-1 for the 6-minute conditioning time points.

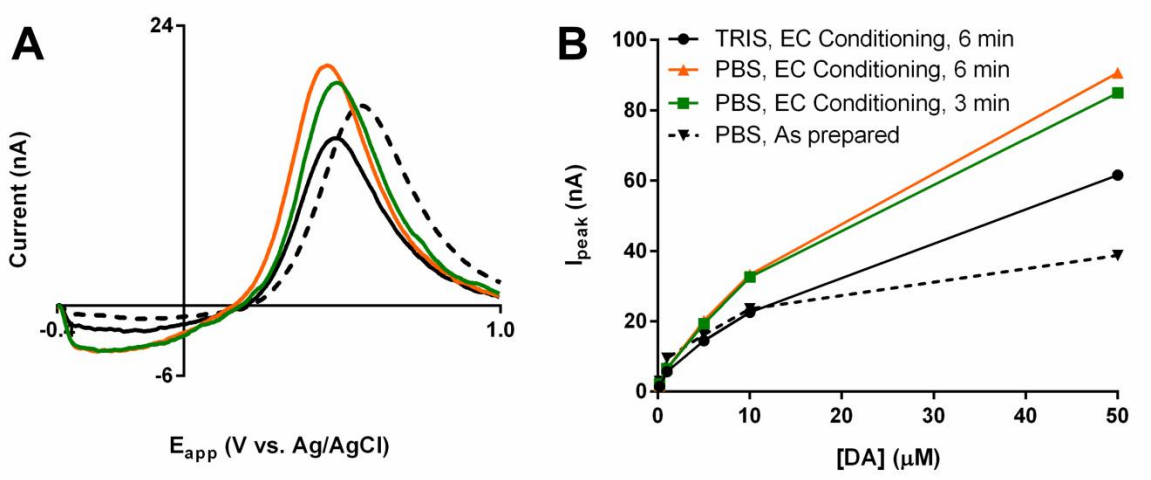

Figure S-3. Background-subtracted FSCV signals for dopamine concentration changes in PBS and TRIS buffer. Representative background-subtracted CVs (A, 500 nM, forward sweep only) and adsorption curves (B) for dopamine injections for as-prepared (solid black) and after 3 and 6 minutes of electrochemical conditioning (green and orange, respectively) in PBS and subsequent change to TRIS buffer (dashed black).

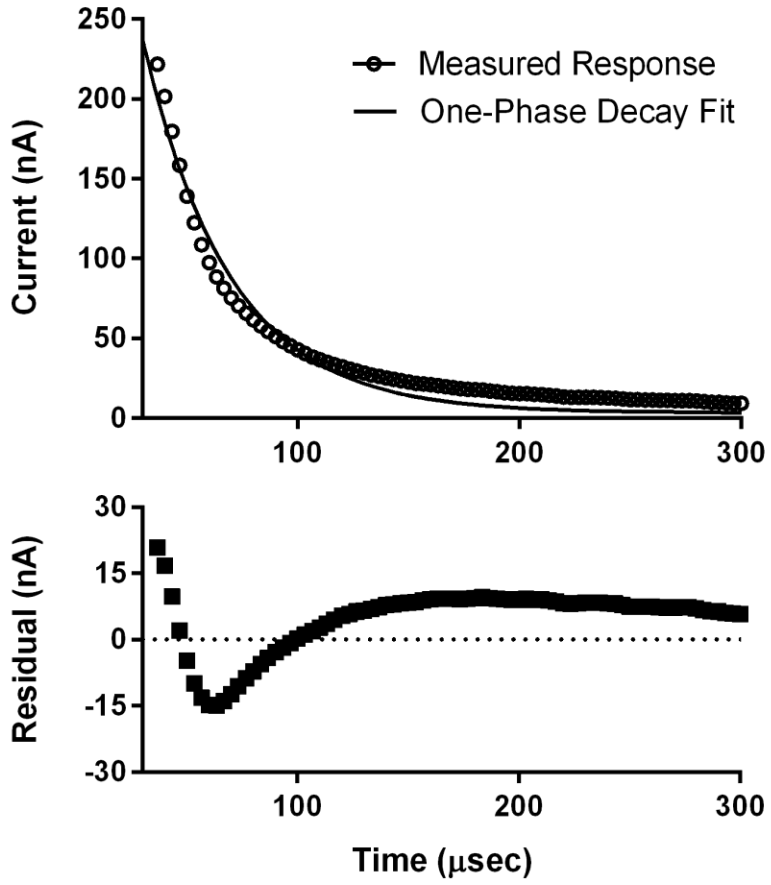

Figure S-4. Results of one-phase exponential decay fit to current response to 40 mV voltage step at carbon-fiber microelectrode. (A) Measured response (empty circles) and exponential fit (line, RC = 39.2 μs) with residual plot (below).

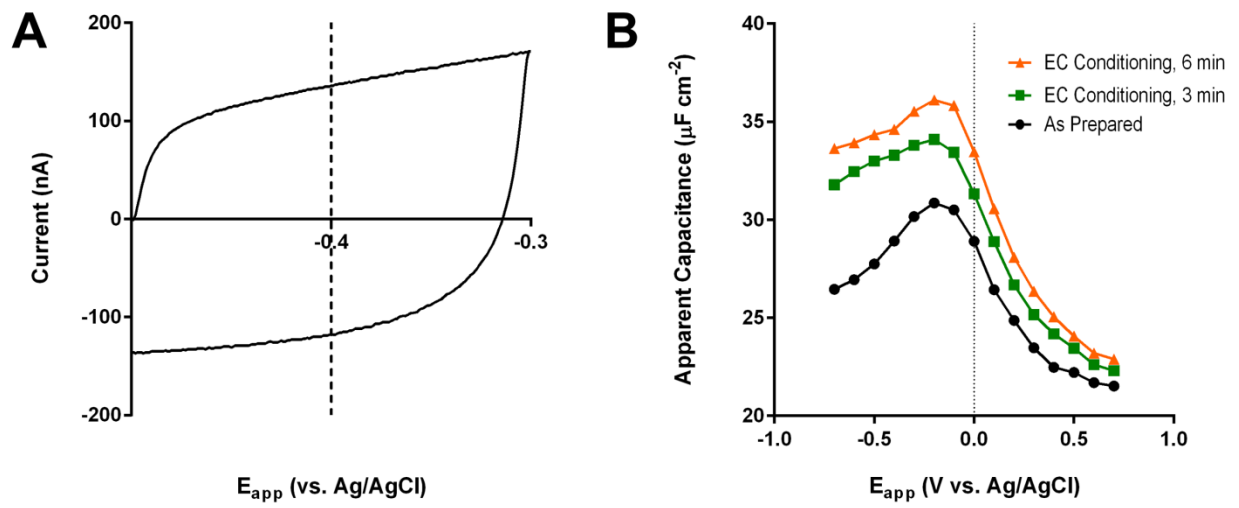

Figure S-5. Voltage-dependent psuedocapacitance determined from small amplitude CVs. (A) Example of small amplitude (200 mV, 200 V/s) anodic CV used to determine pseudocapacitance, done by averaging the absolute values of the two current measurements at a center potential (shown by dashed line) and dividing by scan rate. (B) Pseudocapacitance measurements for as-prepared carbon fiber microelectrodes (black) and after electrochemical conditioning for 3 and 6 minutes (green and orange, respectively).

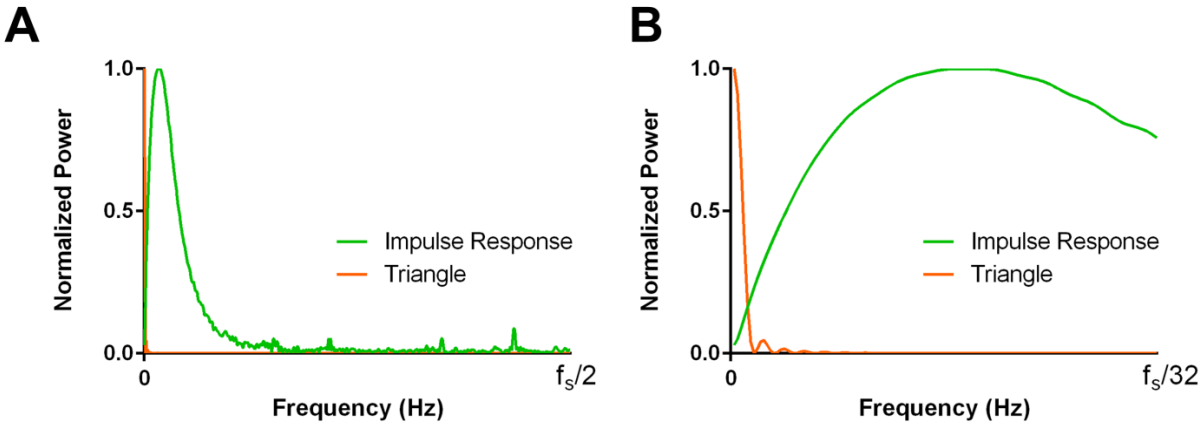

Figure S-6. Power spectra for a triangular voltage wave and a typical impulse response estimation over the entire frequency range (A, zero to half the sampling frequency, f_s – here, 300 kHz) and in the lower frequency range (B, zero to $f_x/32$ – here, 9.375 kHz)

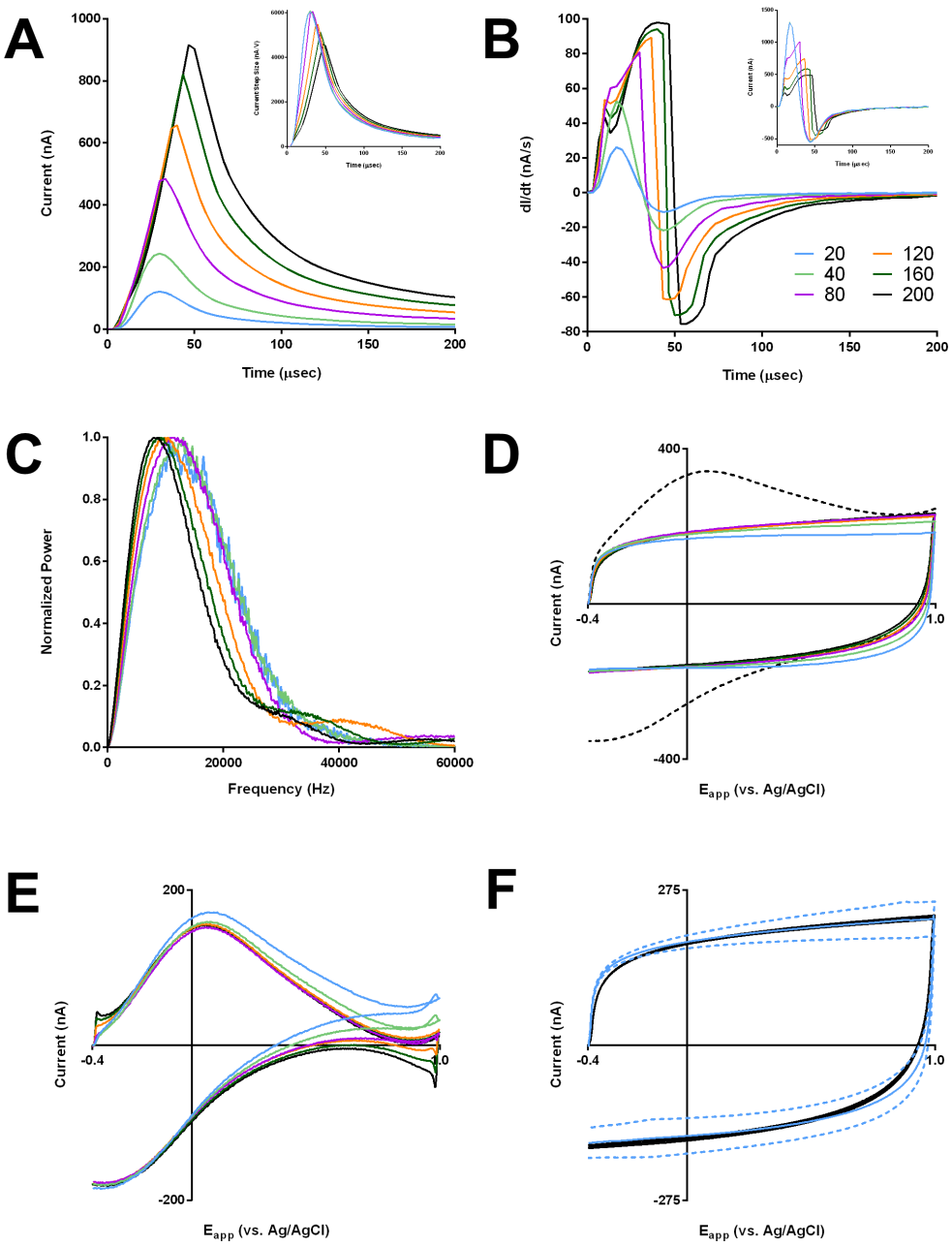

Figure S-7. Effect of step size on prediction for different voltage step amplitudes (20-200 mV) using a low-pass voltage filter (cut-off frequency of 25 kHz) and sampling frequency of 300 kHz. (A) Current response obtained to voltage step, normalized to step height in inset. (B) Impulse response estimations from (A), normalized to step height in inset. (C) Fourier transforms of impulse response estimations from (B). (D) Predictions generated from convolution of impulse response estimations with 400 V/s triangular voltage sweep, with actual response shown as dotted line. (E) Prediction-subtracted voltammograms (actual less prediction) from (D). (F) Average prediction (solid) ± one standard deviation (dotted) estimated from a five-second recording for 20 mV (blue) and 200 mV (black) voltage pulses.

Simulation of Model Background Currents

As stated in the main text, we considered the double layer as a parallel network with a voltage-dependent impedance element (Z_{QH}, corresponding to the quinone-like redox reaction), a voltage-dependent capacitor (C_{QH}, the capacitance arising from species bound to the quinone-like moiety), and a voltage-independent capacitor (C_I).

To model the expected current from Z_{QH}, given a surface-bound, quinone-like species with total surface concentration of Γ_{QH}* that undergoes a two-electron (n = 2), reversible reaction, we expect, from the derivation in Bard and Faulkner, Chapter 14.3.2 for adsorbed species, the following i-E curve for the faradaic couple to application of a voltammetric sweep:

$$i(E) = \frac{n^2F^2}{RT} vA\Gamma_{QH}^* \frac{\left(\frac{b_O}{b_R}\right)\exp[\left(\frac{nF}{RT}\right)(E - E^O))]}{[1 + \left(\frac{b_O}{b_R}\right)\exp[\left(\frac{nF}{RT}\right)(E - E^O))]^2} \quad \text{(Eq. 1)}$$

Since the species is surface-bound, we set the ratio (b_O/b_R) to be 1 for further use.

To model the capacitive charging current, the redox-coupled, area-normalized capacitance (C_{QH}^*, $F \cdot cm^{-2}$) is assumed to be linearly dependent on the surface concentration of both species (Γ_{QH} and Γ_Q, $mol \cdot cm^{-2}$) and respond immediately to their concentration:

$$C_{QH}^*(E) = C_{QH}(E) + C_Q(E) \quad \text{(Eq. 2)}$$

$$C_{QH}^*(E) = b\Gamma_{QH}(E) + c\Gamma_Q(E) \quad \text{(Eq. 3)}$$

$$C_{QH}^*(E) = b\Gamma_{QH}(E) + c(\Gamma_{QH}^* - \Gamma_{QH}(E)) \quad \text{(Eq. 4)}$$

where b and c are constants ($F \cdot mol^{-1}$). To simplify this further, $R_{c/b}$ (the ratio of c to b, assumed to be a constant less than 1) is introduced:

$$C_{QH}^*(E) = b\left[R_{c/b}\Gamma_{QH}^* + \Gamma_{QH}(E)(1 - R_{c/b})\right] \quad \text{(Eq. 5)}$$

Using the Nerst relation, this can be put in terms of the total surface concentration Γ_{QH}*:

$$\Gamma_{QH}(E) = \frac{\Gamma_{QH}^*}{1 + \exp\left[\left(\frac{nF}{RT}\right)(E - E^O)\right]} \quad \text{(Eq. 6)}$$

$$C_{QH}^*(E) = b\Gamma_{QH}^*\left[R_{c/b} + \frac{1 - R_{c/b}}{1 + \exp\left[\left(\frac{nF}{RT}\right)(E - E^O)\right]}\right] \quad \text{(Eq. 7)}$$

Finally, there is the voltage-independent capacitance (C_I), giving a total electrode capacitance (C_{tot}) of:

$$C_T(E) = C_I + C^*_{QH}(E) \quad \text{(Eq. 8)}$$

With this, the i-E curve for the capacitive charging current for application of triangular sweep is expected to be:

$$i = v * C_T(E) * \left[1 - \exp[\frac{-t}{R_S C_T(E)}]\right] \quad \text{(Eq. 9)}$$

where R_s is the solution resistance. Here, it is noted that this equation is applicable for time-independent capacitances; that is:

$$\frac{d(C_T E)}{t} = C_T(E)\left(\frac{dE}{dt}\right) + E\left(\frac{dC_T(E)}{dt}\right) \quad \text{(Eq. 10)}$$

While some contribution from the latter term is anticipated, we expect that term to be considerably smaller than the former at the high scan rates (dE/dt = 400) and moderate applied potentials (-0.8-0.8 V) in this work. Thus, it is ignored. For ease of analysis, we consider the region around the faradaic couple and assume this to be far from the switching potentials, simplifying Equation 9 to:

$$i(E) = vC_I + vC^*_R(E) \quad \text{(Eq. 11)}$$

$$i(E) = vC_I + v\Gamma^*_{QH} b\left[R_{c/b} + \frac{1 - R_{c/b}}{1 + \exp\left[\left(\frac{nF}{RT}\right)(E - E^O)\right]}\right] \quad \text{(Eq. 12)}$$

We introduce $i_{QH,max}{}^*$ indicate the maximum redox-associated charging current (seen at very negative potentials where $\Gamma_{QH}{}^* = \Gamma_{QH} = \Gamma_{QH,max}$, since $r_{b/c}$ is assumed to be less than 1) as well as the constant i_{CI}:

$$i_{CI} = vC_I \quad \text{(Eq. 13)}$$

$$i^*_{QH,max} = vb\Gamma^*_{QH} \quad \text{(Eq. 14)}$$

$$i(E) = i_{CI} + i^*_{QH,max}\left[R_{c/b} + \frac{(1 - R_{c/b})}{1 + \exp\left[\left(\frac{nF}{RT}\right)(E - E^O)\right]}\right] \quad \text{(Eq. 15)}$$

For the study of ionic changes, which are expected to affect primarily the capacitance values, the Faradaic current serves as a useful point of comparison. The equation of the peak current expected for the Faradaic couple ($i_{p,F}$) is also normalized the Faradaic currents:

$$i_{p,F} = \frac{1}{4}\left(\frac{n^2F^2}{RT} * vA\Gamma^*_R\right) \quad \text{(Eq. 16)}$$

$$\frac{i(E)}{i_{p,F}} = 4\frac{\exp[\left(\frac{nF}{RT}\right)(E - E^O))]}{[1 + \exp[\left(\frac{nF}{RT}\right)(E - E^O))]^2} \quad \text{(Eq. 17)}$$

The total expected potential-dependent current (i_T, normalized to $i_{p,F}$) is then simply the summation of these two contributions at a given values of three constants - I_C (i_{CI} /$i_{p,F}$), I_{QH} ($i_{QH,max}{}^*$/$i_{p,F}$) , and $R_{c/b}$:

$$\frac{i_T(E)}{i_{p,F}} = I_C + I_{QH}\left[R_{c/b} + \frac{(1 - R_{c/b})}{1 + \exp\left[\left(\frac{nF}{RT}\right)(E - E^O)\right]}\right] + 4\left[\frac{\exp[\left(\frac{nF}{RT}\right)(E - E^O))]}{[1 + \exp[\left(\frac{nF}{RT}\right)(E - E^O))]^2}\right] \quad \text{(Eq. 18)}$$

For values of I_C = 1, I_{QH} = 2, and $R_{b/c}$ = 0.5, this gives the current-potential curves shown in Figure S-8.

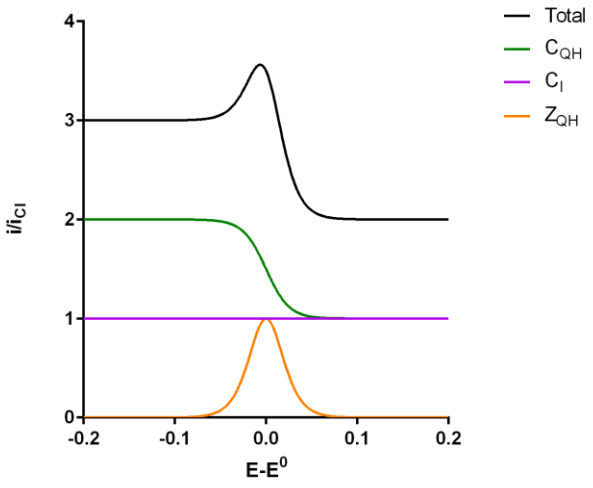

Figure S-8. Model-simulated voltammetric currents for the components of the carbon-fiber double layer.